Carbohydrate Polymers 273 (2021) 118541

Contents lists available at ScienceDirect

Carbohydrate Polymers

journal homepage: www.elsevier.com/locate/carbpol

# Enhanced blood coagulation and antibacterial activities of carboxymethyl-kappa-carrageenan-containing nanofibers

Liszt Y.C. Madruga [a,b], Ketul C. Popat [c,d,e], Rosangela C. Balaban [b], Matt J. Kipper [a,c,e,*]

[a] Department of Chemical and Biological Engineering, Colorado State University, Fort Collins, CO, United States
[b] Institute of Chemistry, Federal University of Rio Grande do Norte (UFRN), Natal, RN, Brazil
[c] School of Advanced Materials Discovery, Colorado State University, Fort Collins, CO, United States
[d] Department of Mechanical Engineering, Colorado State University, Fort Collins, CO, United States
[e] School of Biomedical Engineering, Colorado State University, Fort Collins, CO, United States

ARTICLE INFO

*Keywords:*
Carboxymethyl-kappa-carrageenan
Polysaccharides
Platelet adhesion
Protein interaction
Antibacterial activity
Wound dressings

ABSTRACT

Ideal wound dressings should be biocompatible, exhibit high antibacterial activity, and promote blood coagulation. To impart these imperative functions, carboxymethyl-kappa-carrageenan was incorporated into poly (vinyl alcohol) nanofibers (PVA-CMKC). The antibacterial activity of the nanofibers was evaluated. Adsorption of two important blood proteins, fibrinogen and albumin, was also assessed. The adhesion and activation of platelets, and the clotting of whole blood were evaluated to characterize the ability of the nanofibers to promote hemostasis. Adhesion and morphology of both *Staphylococcus aureus* and *Pseudomonas aeruginosa* were evaluated using fluorescence microscopy and scanning electron microscopy. CMKC-containing nanofibers demonstrated significant increases in platelet adhesion and activation, percentage of coagulation in whole blood clotting test and fibrinogen adsorption, compared to PVA nanofibers, showing blood coagulation activity. Incorporating CMKC also reduces adhesion and viability of *S. aureus* and *P. aeruginosa* bacteria after 24 h of incubation. PVA-CMKC nanofibers show potential application as dressings for wound healing applications.

## 1. Introduction

Skin is an important barrier, providing protection from bacterial infection and environmental damage (Mogoşanu & Grumezescu, 2014). Skin damage caused by burns, chemicals, and accidents can lead to wounds with delayed healing and elevated risk of infection. (Dumont et al., 2018). However, wound healing is a complex sequence involving multiple cell types, which is coordinated by dynamic cytokine signalling. Wound dressings that promote wound healing and prevent infection are an essential resource for wound treatment.

Wound dressings represent a significant component of the healthcare market (Homaeigohar & Boccaccini, 2020). Ideal wound dressings should be biocompatible and should support the healing process, while preventing bacterial infection. Wound dressings should also provide stable coverage, promote coagulation of the blood to accelerate closure of the wound, absorb wound exudate while maintaining moisture, and exhibit low adherence to the wound surface, enabling removal without causing additional trauma (Chattopadhyay & Raines, 2014).

Many currently available wound dressings are films, foams, and hydrogels (Almodóvar et al., 2013; Bajpai & Daheriya, 2014; da Cruz et al., 2020; Das et al., 2019; Fujiwara et al., 2012; Yegappan, Selvaprithiviraj, Amirthalingam, & Jayakumar, 2018; Zia et al., 2017). Nanofibrous materials have emerged as new wound dressings, due to their notably large exposed surface area and nanoporosity, normally on the scale of nanometers. These characteristics can mimic the extracellular matrix (ECM) structure, facilitating interactions with cells in the wound bed (Bhattacharjee, Clark, Gentry-Weeks, & Li, 2020; Guo et al., 2016; Sadeghi, Zandi, Pezeshki-Modaress, & Rajabi, 2019; Truong, Glattauer, Briggs, Zappe, & Ramshaw, 2012; Unnithan et al., 2015; Xu, Weng, Gilkerson, Materon, & Lozano, 2015). Electrospinning is a well-established technique for the production of nanoscale fibers. Electrospun nanofibers comprise highly porous 3D structures, that enhance cell-material and cell-cell interactions, while maintaining or enhancing the biological properties of the material used for nanofiber preparation. Moreover, the simplicity and low operating cost make electrospinning a compelling method for production of nanostructured materials (Madruga, Balaban, Popat, & Kipper, 2021; Mogoşanu & Grumezescu, 2014). Electrospun nanofibers can be modified to incorporate biological

* Corresponding author at: Department of Chemical and Biological Engineering, Colorado State University, Fort Collins, CO, United States.
*E-mail address:* matthew.kipper@colostate.edu (M.J. Kipper).

https://doi.org/10.1016/j.carbpol.2021.118541
Received 21 May 2021; Received in revised form 3 August 2021; Accepted 5 August 2021
Available online 11 August 2021

signals that promote healing. However, incorporation of all functions necessary to promote wound healing into synthetic polymers increases the complexity and cost of the process, reducing manufacturability. On the other hand, natural polymers with inherent biocompatibility and biological activities, combined with the favorable wound healing properties introduced via electrospinning can overcome many of these challenges (de Oliveira et al., 2021; do Nascimento Marques et al., 2020; Miguel et al., 2018; Zahedi, Rezaeian, Ranaei-Siadat, Jafari, & Supaphol, 2010; Zhao et al., 2014).

Nanofibers can be prepared from natural polymers that possess similar chemical compositions to components of the extracellular matrix, facilitating the manufacture of fibers similar to the ECM (Young et al., 2017). Nanofiber-based dressings for wound healing should possess favorable biological properties, including cytocompatibility, moisture retention, blood coagulant activity, antibacterial activity, non-toxicity, and low cost (Fahimirad & Ajalloueian, 2019; Felgueiras & Amorim, 2017; Haider, Haider, & Kang, 2018; Nas, Abrigo, McArthur, & Kingshott, 2014; Trinca, Westin, da Silva, & Moraes, 2017; Zia et al., 2017).

Carrageenan and derivatives of carrageenan are attractive biomaterials. Carrageenans are sulfated polysaccharides, affording the opportunity to introduce biochemical functionality of sulfated polymers, without requiring harsh and hazardous sulfation/sulfonation chemistries. Previous work from our labs has shown that carboxymethyl kappa-carrageenan (CMKC) exhibits high cell viability, no cytotoxicity toward human adipose-derived stem cells (ADSCs), and no hemolytic activity toward human red blood cells. Furthermore, these materials exhibit increased antioxidant activity and they inhibit *Staphylococcus aureus*, *B. cereus*, *E. coli*, and *P. aeruginosa* (Madruga et al., 2020).

Electrospinning of CMKC is difficult because it is a strong polyelectrolyte. Therefore, we blended CMKC with poly(vinyl alcohol) (PVA) to form PVA-CMKC aqueous solutions, to improve the spinnability of CMKC, and successfully produced nanofibers. Both PVA and CMKC are hydrophilic, making the electrospun fibers water soluble as well, and therefore unsuitable for wound dressing applications, since they need to be able to absorb the exudate of the wounds. Thermal crosslinking for 8 h at 180 °C induces ester bond formation between carboxyl groups in CMKC and hydroxyl groups in PVA making them insoluble in water (Madruga, Balaban, Popat, & Kipper, 2021). The CMKC-containing nanofibers exhibit high cytocompatibility, cell growth and cell adhesion of ADSCs, biodegradability in a lysozyme solution, and enhanced ADSC response with respect to osteogenic differentiation (Madruga, Balaban, Popat, & Kipper, 2021). These properties suggest that CMKC-containing nanofibers are excellent candidate biomaterials for tissue engineering. However, the hemostatic property and antibacterial activity of these nanofibers, which are important properties for wound healing, have not been reported.

Based on our previous work, we hypothesize that antimicrobial activity and procoagulant activity can be introduced into nanofibers by blending CMKC with PVA. In this work, we evaluated the antibacterial activity and blood protein interactions with PVA-CMKC electrospun nanofibers (0, 25, 50 and 75 wt.% CMKC). In this work, the nanofibers were exposed to protein solutions (fibrinogen and albumin), platelet-rich plasma (PRP), human whole blood, and bacteria inocula. Protein adsorption was evaluated by X-ray photoelectron spectroscopy (XPS). The amount of adhered platelets and blood clotting index were analysed by scanning electron microscopy (SEM), fluorescence microscope images, and absorbance measures. The adhesion and cellular integrity of *S. aureus* and *P. aeruginosa* on the nanofibers were evaluated by SEM images and fluorescence microscope images using live/dead staining. PVA-CMKC nanofibers may have improved features and functions compared to other wound dressing formulations (e.g., hydrogels), such as increased surface area, nanoscale topographic features, the ability to absorb the exudate of the wounds, hemostatic activity, and antibacterial activity. PVA-CMKC nanofibers may therefore be used as dressings for wound healing applications.

## 2. Experimental section

### 2.1. Materials

Poly(vinyl alcohol) 87–89% hydrolyzed (PVA) of $M_w$ 1.46–1.86 × $10^5$ g $mol^{-1}$, kappa-carrageenan (KC) of $M_w$ 3.9 × $10^5$ g $mol^{-1}$ [determined previously by our group (Madruga, da Câmara, Marques, & Balaban, 2018)] and monochloroacetic acid (MCA) were purchased from Sigma-Aldrich (USA). LB broth (Miller) was purchased from Fisher (USA). Millipore water was used in the preparation of all aqueous solutions.

### 2.2. Carboxymethylation of kappa-carrageenan

Williamson's ether synthesis procedure was followed to carboxymethylate KC, according to previous protocols (Madruga et al., 2020; Madruga, Balaban, Popat, & Kipper, 2021). Briefly, KC (10 g) was suspended in an aqueous solution (200 mL) containing 80% (w/v) of 2-propanol in a three-necked glass flask coupled with a reflux condenser. A 20% (w/v) NaOH aqueous solution (20 mL) was added dropwise over 15 min. The reaction mixture was kept at 40 °C for 1 h with vigorous stirring. A solution of monochloroacetic acid (8.75 g in 20 mL of 20% NaOH aqueous solution) was added dropwise with a syringe over 20 min to the KC solution, and the temperature was maintained at 55 °C for 4 h with stirring. The product was recovered through vacuum filtration and washed three times with 80% 2-propanol aqueous solution and pure 2-propanol. The precipitate was dissolved in deionized water (300 mL) overnight. The solution was dialyzed against water through a membrane (7000 Da maximum molecular weight cutoff) until the conductivity was below 20 mS·$cm^{-1}$, measured with a conductivity meter from Thermo Orion, model Orion 145A+, with conductivity cell Orion 011510 (USA). Finally, the material was freeze-dried in a ModulyoD lyophilizer from ThermoSavant. The reaction was conducted with the molar ratio of MCA:KC monomer of 3.5:1, yielding CMKC with a degree of substitution (DS) of 1.1 ($M_w$ 4.3 × $10^5$ g $mol^{-1}$). This DS was chosen based on our previous evaluation of different CMKC DS and biological assays (Madruga et al., 2020; Madruga, Balaban, Popat, & Kipper, 2021). The modified KC is referred to as carboxymethyl-kappa-carrageenan (CMKC).

### 2.3. Electrospinning of PVA-CMKC nanofibers

Nanofibers were fabricated by electrospinning following procedures from our previous report (Madruga, Balaban, Popat, & Kipper, 2021). Briefly, the solutions were prepared by blending PVA and CMKC at different weight ratios in water (5.0 mL) and stirring overnight. The CMKC content (wt%) is reported relative to the total polymer concentration (which is 5% w/v for all samples) in the final solution. Four compositions were used in this study, with 0, 25, 50 and 75 wt% CMKC. The blend solutions were pumped (at 1.0 mL $h^{-1}$ for 5 h), using a syringe pump (Genie Plus, Kent Scientific, Torrington, CT), through a 19-gauge needle (0.686 mm inner diameter). Electrospinning was carried out at ambient conditions (19 ± 1 °C and 18% relative humidity), at a field strength of 1 kV $cm^{-1}$ provided by a DC power supply (Gama High Voltage Research, Ormond Beach, FL). Nanofibers were collected on aluminum foil on a copper plate. The nozzle-to-collector distance was set as 15 cm. The nanofibers were cut into 8-mm diameter circles for all subsequent assays. For crosslinking, heat treatment of the nanofibers in a vacuum oven at 180 °C for 10 h was performed (Madruga, Balaban, Popat, & Kipper, 2021).

### 2.4. Characterization of PVA-CMKC nanofibers

Nanofiber chemical composition was characterized by X-ray photoelectron spectroscopy (XPS) (5800 spectrometer, Physical Electronics, Chanhassen, MN). Survey spectra were collected from 0 to 1100 eV, with

**Table 1**
Elemental composition of the nanofibers.

| | % C1s | % N1s | % O1s | % S2p |
|---|---|---|---|---|
| PVA | 70.53 | 0.00 | 29.47 | 0.00 |
| PVA-CMKC 25% | 66.78 | 0.00 | 32.79 | 0.43 |
| PVA-CMKC 50% | 60.99 | 0.00 | 38.50 | 0.51 |
| PVA-CMKC 75% | 65.15 | 0.00 | 34.18 | 0.67 |

a pass energy of 187 eV. The C1s peak (284.8 eV) was used as reference. High-resolution spectra of the C1s envelopes were also acquired with 0.1 eV steps and an X-ray spot of 800 μm. Origin and Multipak Software were used for performing the curve fitting of all presented spectra.

### 2.5. Hemostatic activity

#### 2.5.1. Protein adsorption on the nanofibers

The adsorption of fibrinogen (FIB) and albumin (ALB) to nanofibers was investigated following the procedure reported previously (da Câmara et al., 2020; Sabino et al., 2020; Sabino, Kauk, Movafaghi, Kota, & Popat, 2019). The nanofibers were sterilized by immersion in 70% ethanol for 15 min and washed 3 times with sterile phosphate-buffered saline (PBS). Sterilized nanofibers were incubated in a 48-well plate with 100 μg $mL^{-1}$ solution of human fibrinogen or albumin at 37 °C for 2 h with 100 rpm shaking. All samples were rinsed with PBS and water before analysis. The surface composition of adsorbed samples before and after protein adsorption was characterized by the C1s envelope using high-resolution XPS spectra, by evaluating the C—N peaks.

#### 2.5.2. Platelet adhesion and activation

For this study two healthy individuals consented to donate blood via venous phlebotomy, using procedures approved by the Colorado State University Institutional Review Board, in accordance with the National Institutes of Health's "Guiding Principles for Ethical Research." Blood was drawn by a phlebotomist (into 10 mL EDTA-coated vacuum tubes). Whole blood was centrifuged (100 ×*g* for 15 min). The plasma containing the platelets and leukocytes was removed and allowed to rest for 10 min before use, to obtain platelet-rich plasma (PRP). Fluorescence microscopy was used to evaluate the platelet adhesion on the nanofibers (da Câmara et al., 2020; Sabino et al., 2020). Six separate samples of each nanofiber were used for fluorescence microscopy. Each sample was placed in the well of a 48-well plate and incubated with 500 μL of PRP (37 °C for 2 h with 100 rpm shaking). Following incubation with PRP, samples were rinsed with PBS and water before analysis, to remove non-adhered platelets. The samples were then stained with calcein-AM live stain (Invitrogen) in PBS (2 μM) for 30 min with 100 rpm shaking at room temperature, protected from light. The samples were imaged using a Zeiss Axiovision fluorescence microscope using a 493/514 nm filter, and five images from randomly selected locations were taken from each of three samples per condition. ImageJ software was used to calculate the percentage of the area with adhered platelets.

Platelet activation was also characterized by scanning electron microscopy (SEM) on three separate samples of each nanofiber type. The nanofibers were incubated for 2 h in PRP, then rinsed twice with PBS and were fixed with primary fixative (3.0% glutaraldehyde, 0.1 M sodium cacodylate, and 0.1 M sucrose) for 45 min. Primary fixation was followed by a 10-min secondary fixation (using primary fixative without glutaraldehyde). After fixation, the nanofibers were dehydrated with consecutive solutions of ethanol (35, 50, 70, and 100%, respectively) for 10 min each. All samples were sputter-coated with gold (15 nm) and imaged via SEM (JSM-6500F JEOL, Tokyo, Japan) using an accelerating voltage of 15 kV. Five images of randomly selected locations were taken from each of three samples per condition. The SEM images were used to visualize platelet adhesion and morphology, indicative of platelet activation.

#### 2.5.3. Whole blood clotting

Human blood from healthy donors was drawn into 3 mL vacuum tubes with no anticoagulants by a trained phlebotomist. To evaluate whole blood clotting kinetics, sterilized nanofiber samples were placed in a 24-well plate and 5.0 μL of whole blood was dropped on each sample and allowed to clot for 15 and 30 min. In a different 24-well plate, with 500 μL DI water, the nanofibers were gently agitated for 5 min on a shaker to lyse the red blood cells and release free hemoglobin. The absorbance of free hemoglobin was measured using a plate reader (Molecular Devices Spectra Max M3) at 540 nm. The control for 100% free hemoglobin was obtained from a sample solubilized in water and measured immediately after collection (0 min) (da Câmara et al., 2020; Sabino & Popat, 2020).

### 2.6. Antibacterial activity

A standardized inoculum of each strain (*Pseudomonas aeruginosa* P01 and *Staphylococcus aureus* ATCC 6538) was prepared by suspending colonies directly in a nutrient broth media solution (LB-Miller — 25 mg $mL^{-1}$) diluted to obtain a concentration of $10^6$ CFU/mL. To evaluate the antibacterial activity, 500 μL of bacteria solution was added to the sterilized nanofibers for 6 and 24 h.

#### 2.6.1. Bacteria adhesion and morphology on the nanofibers

The adhesion of live and dead bacteria to the nanofibers was evaluated using a live/dead stain (3 μL/mL of propidium iodide and Syto 9 stain 1:1 in PBS), following the protocol of the manufacturer, and quantified from fluorescence microscope images. The nanofibers were rinsed with PBS three times after the incubation period, and the stain solution was added and allowed to react with the samples for 20 min. Then the nanofibers were rinsed with PBS and imaged on a Zeiss Axiovision fluorescence microscope. The percentage of live and dead bacteria on the nanofibers was determined by analyzing the fluorescence microscopy images in ImageJ. Five images from randomly selected locations were taken from each of three samples per condition.

Scanning electron microscopy was used to investigate the morphology of the adhered bacteria and biofilm formation on the nanofibers. After incubation for 6 and 24 h in bacteria broth, the nanofibers were rinsed with PBS to remove non-adhered bacteria. The samples were fixed and dehydrated as described above for the platelet SEM images (Section 2.5.2).

### 2.7. Statistical analysis

At least three different samples of each nanofiber type were used in all experiments; results are presented as mean ± standard deviation. Differences were determined using one-way ANOVA ($p = 0.05$) with a post-hoc Tukey's honest significant difference test.

## 3. Results and discussion

### 3.1. Characterization of PVA/CMKC nanofibers

The SEM images agree with the fiber morphology of our previous study, showing that the thermal crosslinking maintains the morphology of all nanofibers and makes them insoluble in water (Fig. S1 in the supplementary information).

XPS data confirm the chemical composition of the crosslinked nanofibers. Survey spectra of the nanofibers have oxygen (O1s) and carbon (C1s) peaks, and CMKC-PVA nanofiber spectra also have sulfur (S2s and S2p) peaks, from the sulfate groups in CMKC (Fig. S2 — supplementary information). From survey XPS scans, elemental composition of the nanofibers was obtained, and the data are shown in Table 1. The CMKC-containing nanofibers have increasing sulfur content with increasing concentration of CMKC in the samples. High-resolution XPS C1s spectra were also collected (Fig. 1a). The CMKC-containing

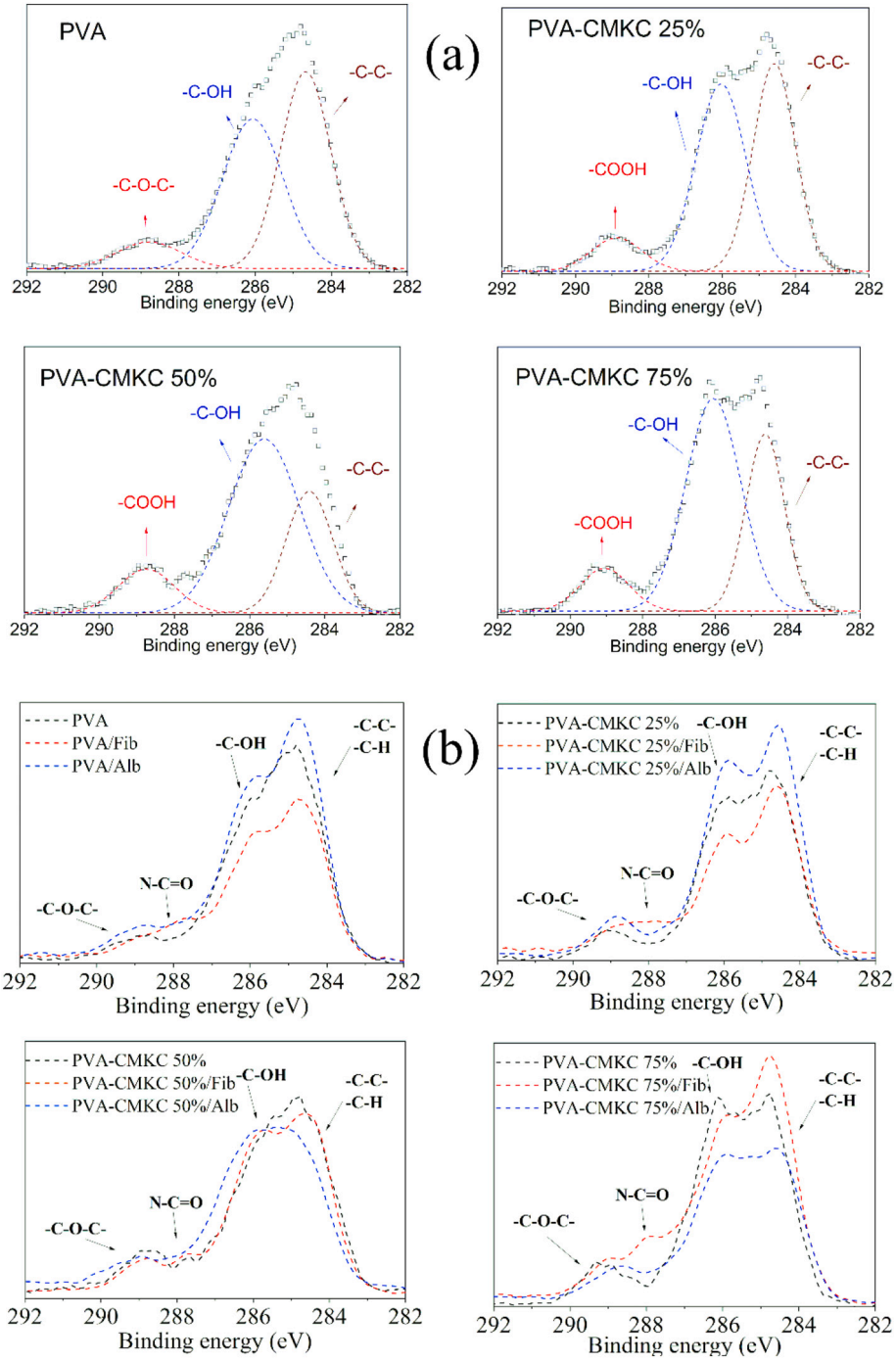


**Fig. 1.** XPS high-resolution C1s spectra for crosslinked nanofibers (a); high-resolution C1s spectra for FIB and ALB adsorbed on nanofibers showing C—H, C—C, C—OH, N—C═O and C—O—C signals (b).

nanofibers have a significant increase in –COOH groups, compared to the PVA nanofibers, due to the presence of the carboxymethyl group on CMKC. The crosslinked nanofibers contain ether and ester bonds resulting in peaks in the region of 286 eV and overlap with the C—OH bonds. However, previously reported infrared spectra confirmed the presence of the crosslinked sites with peaks between 1700 and 1750 $cm^{-1}$ (Madruga, Balaban, Popat, & Kipper, 2021). The incorporation of CMKC is therefore confirmed by the XPS spectra and agrees with the FTIR data from our previous study.

### 3.2. Hemostatic activity

#### 3.2.1. Protein adsorption on the nanofibers

Blood clot formation results from the activation and aggregation of platelets, and a multistep coagulation cascade, culminating with the polymerization of fibrinogen and formation of a network of crosslinked fibrin fibers (Hedayati, Neufeld, Reynolds, & Kipper, 2019). The monolayer of proteins that adsorbs on the surface of a biomaterial is a mediator to the formation of a clot, and its composition can dictate subsequent biological protein processes (Prawel et al., 2014). Albumin (ALB) is one of the most abundant proteins in the blood. Albumin adsorption can block or promote coagulation, depending on whether it is

**Table 2**
Nitrogen content of the nanofibers before and after protein adsorption experiments, obtained from XPS survey scans.

| | % N (before) | % N (fibrinogen) | % N (albumin) |
|---|---|---|---|
| PVA | 0.00 | 5.28 | 3.03 |
| PVA-CMKC 25% | 0.00 | 3.38 | 1.83 |
| PVA-CMKC 50% | 0.00 | 4.69 | 0.17 |
| PVA-CMKC 75% | 0.00 | 3.13 | 0.61 |

in its native conformation or denatured (Paar et al., 2017). Fibrinogen (FIB) is spindle or rod-shaped protein that is converted to the polymerizable form, fibrin, in the blood coagulation cascade. As the precursor of the polymerizable fibrin, FIB is essential for the formation of blood clots and provides binding sites for platelets (da Câmara et al., 2020; Sabino, Kauk, Movafaghi, Kota, & Popat, 2019).

High-resolution XPS spectra of the C1s envelope and survey spectra were obtained for the nanofibers after incubation in human albumin and fibrinogen solutions. The amount of proteins adsorbed to the nanofibers was estimated by the elemental composition. Since the nanofibers have no nitrogen in their structure (Table 1), the increase in nitrogen elemental composition obtained from the XPS survey scans on the fibers is evidence of protein adsorption (Table 2). The adsorption of FIB and ALB on the fibers was evaluated from the high-resolution spectra for the C1s envelope by analyzing the increment of the amide carbonyl (N—C═O) peaks (Fig. 1b).

FIB promotes platelet adhesion and activation, by exposing binding sites to platelets. Thus, an increase in the adsorption of fibrinogen on the nanofibers can be correlated with increasing pro-coagulant capacity. ALB, on the other hand, can block or promote the formation of clots, depending on the conformation adopted or denaturation. The high-resolution XPS spectra of the C1s envelope (Fig. 1b) shows similar amide peak (N—C═O) increases following adsorption of both proteins to PVA nanofibers. PVA-CMKC nanofibers all exhibit larger nitrogen content increases following fibrinogen adsorption compared to albumin adsorption. PVA nanofibers have the highest nitrogen content following FIB adsorption. The same trend is observed when comparing the amide peak in the C1s spectra for both the PVA-CMKC 25% and 75% (Fig. 1b). This suggests that adding CMKC to nanofibers may promote higher coagulation and blood clot formation, due to higher protein adsorption. Even after crosslinking, all nanofibers still present some hydrophilicity, however, the nanofibers containing CMKC present more crosslinking sites, due to presence of the carboxymethyl groups, which make them a little more hydrophobic when compared to pure PVA. The pure PVA nanofibers had the highest amount of proteins adsorbed, which can be attributed to the high surface area of this fiber and to the hydroxyl and ester groups that can promote protein adsorption and changes in protein conformation (Sivaraman & Latour, 2010; Yang, Han, Liu, Xu, & Jia, 2017). The high adsorption of albumin in PVA nanofibers might block platelet adhesion decreasing clot formation, and the hydrophilicity can lead to a decrease of the platelet binding sites of the fibrinogen adsorbed (Zhang et al., 2017). On the other hand, increasing the concentration of CMKC in the nanofibers up to 50% decreases the albumin adsorption and increases the fibrinogen adsorption, which promotes more sites for platelets to bind and form clots. The chemical similarity of CMKC to biological molecules, such as glycosaminoglycans found in the human body, as well as the large number of hydrogen-bonding groups present on the molecule may promote protein-material interactions (Rodrigues, Gonçalves, Martins, Barbosa, & Ratner, 2006). The PVA-CMKC 75% nanofibers had less fibrinogen and more albumin adsorbed when compared to the PVA-CMKC 50% nanofibers, which could lead to reduced platelet adhesion and activation. The smaller amount of proteins adsorbed can be correlated to the higher dispersity in the fiber diameter, due to the higher instability when electrospinning high charge-density solutions (Haider, Haider, & Kang, 2018; Merkle et al., 2015a).

### 3.2.2. *Platelet adhesion and activation*

Platelet adhesion on the surfaces of biomaterials is an indicator of thrombogenicity and pro-coagulant activity, leading to platelet activation, which can initiate the coagulation cascade (Hedayati, Neufeld, Reynolds, & Kipper, 2019). Fig. 2 illustrates the adhesion of platelets (green) on the surface of the nanofibers and tissue culture polystyrene (control) following 2 h incubation in human PRP. Nanofibers exhibit a

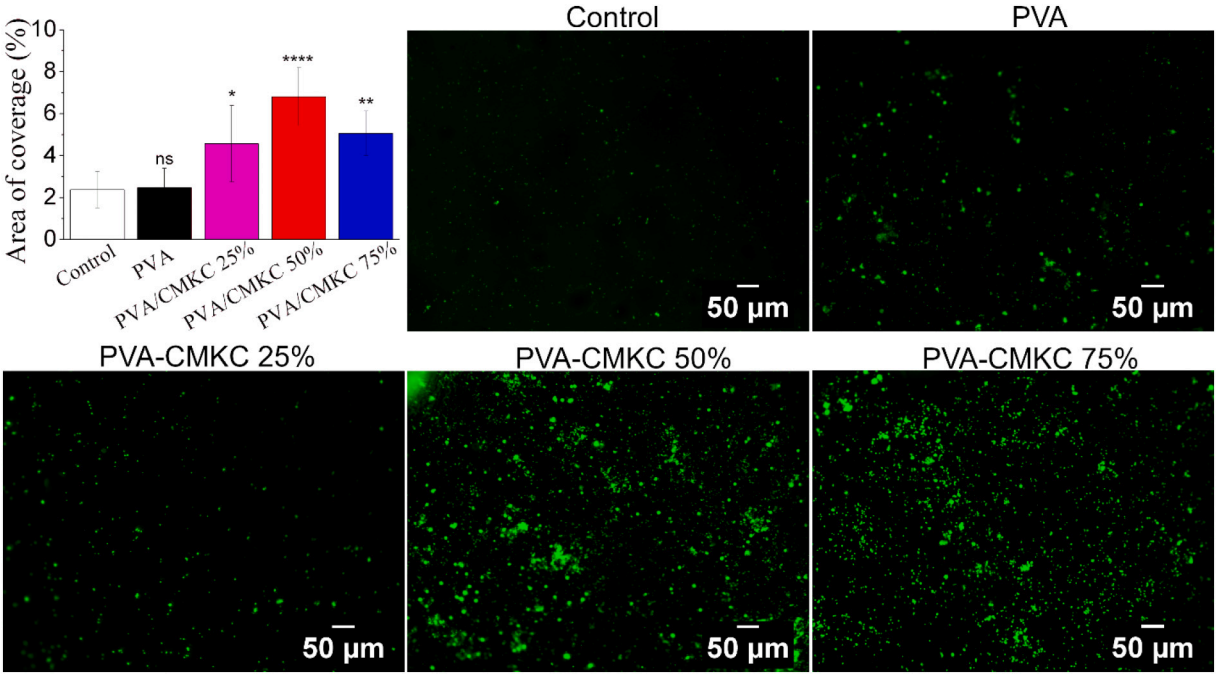


**Fig. 2.** Percentage area of adhered platelets on nanofibers and fluorescence microscopy images of adhered platelets stained with calcein-AM on the nanofibers after 2 h of incubation in platelet-rich plasma. CMKC-containing nanofibers have significantly higher platelet adhesion compared to control. ****$p \leq 0.0001$, **$p \leq 0.01$, *$p \leq 0.05$ and "ns" $p \geq 0.05$.

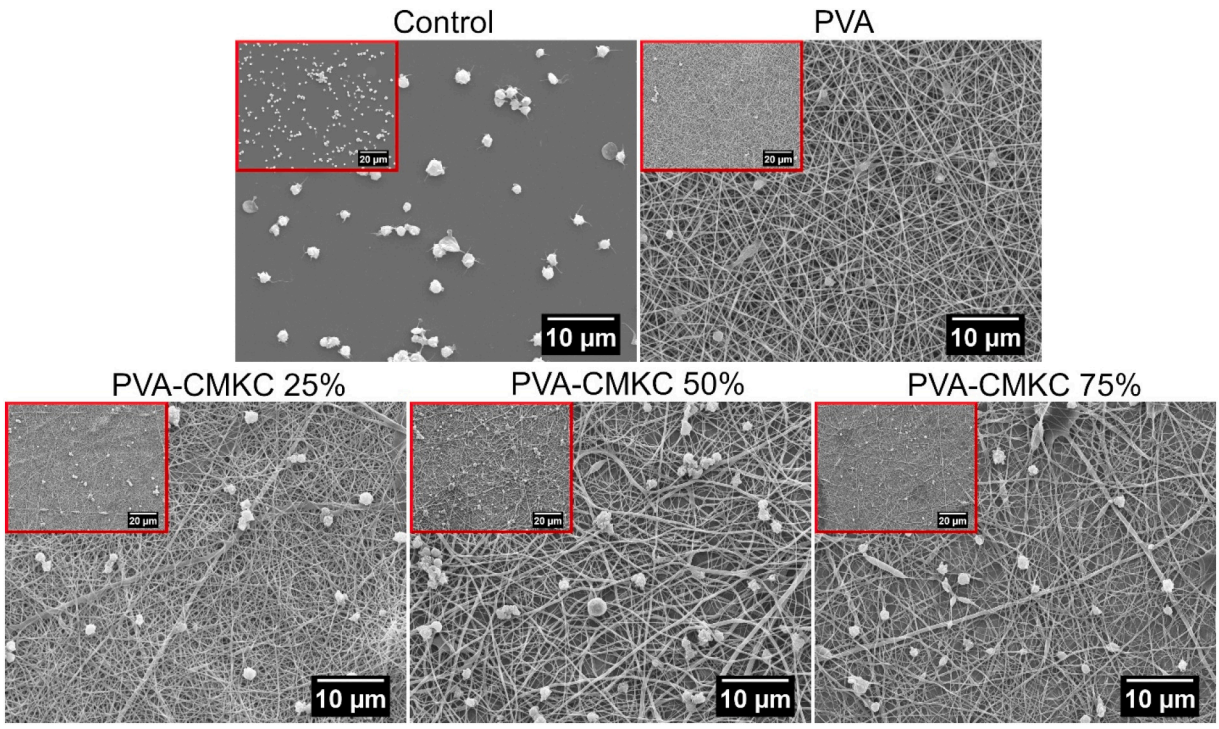


**Fig. 3.** SEM micrographs of adhered platelets on the nanofibers after 2 h of incubation in platelet-rich plasma.

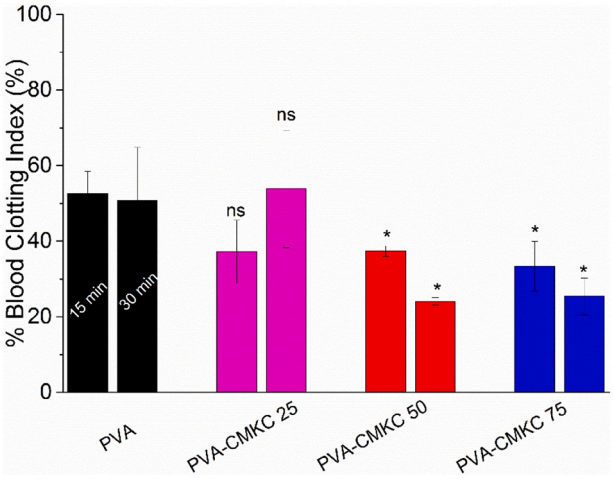


**Fig. 4.** Whole blood clotting measured by the normalized amount of free hemoglobin in human whole blood incubated with nanofibers for 15 and 30 min. Reduced blood clotting index indicates increased clotting. * $p \leq 0.05$ and "ns" $p \geq 0.05$ compared to the PVA control.

significant increase in platelet adhesion compared to the control, which increases with increasing CMKC content. The difference in the number of adhered platelets between the fibers and the control can be attributed partially to the relatively high specific surface area and nanoscale topography of the nanofibers compared to the two-dimensional control surface. Because they have a three-dimensional structure and a rough surface with pores, nanofibers tend to have a higher deposition of platelets and proteins on their surfaces (Zeng et al., 2016). Moreover, when compared with PVA nanofibers, CMKC-containing nanofibers also have higher platelet adhesion (Fig. 2). This suggests that CMKC enhances platelet adhesion. The formation of ester groups by crosslinking with PVA may also contribute to increased platelet adhesion (Ma et al., 2015; Madruga et al., 2020).

Platelet adhesion to surfaces can lead to rapid platelet activation. Activated platelets undergo a series of morphological changes, including spreading, dendrite formation and then aggregation (da Câmara et al., 2020; Sabino, Kauk, Movafaghi, Kota, & Popat, 2019). While non-activated platelets are spherical, platelets undergoing activation exhibit long, finger-like extensions. Fully activated platelets are characterized as having a "fried egg" appearance (Simon-Walker et al., 2017; Vlcek, Hedayati, Melvin, Reynolds, & Kipper, 2021). The morphology of the platelets adhered on the nanofibers was evaluated by SEM images (Fig. 3). The high number of adhered platelets on the CMKC-containing nanofibers seen in the SEM images confirms the observations in the fluorescence micrographs, demonstrating that CMKC promotes platelet adhesion. All platelets show dendrite formation and a very small number are in a round (unactivated) morphology. Heparin, another sulphated polysaccharide can have anticoagulant activity, through interactions with antithrombin III and other components of the coagulation cascade. Nonetheless, when adsorbed to a surface heparin can also promote platelet activation on nanostructured surfaces, as its negatively charged sulfate groups form complexes with positively charged platelet factor 4, which can result in immune complexes that activate platelets (Krauel, Hackbarth, Fürll, & Greinacher, 2012; Vlcek, Hedayati, Melvin, Reynolds, & Kipper, 2021).

Platelets have negatively charged membranes. Since the CMKC is also negatively charged, electrostatic forces alone would cause CMKC to repel platelets from the nanofibers. However, this is not what is observed from the results on Fig. 2. In fact, studies have shown that carboxyl groups, which are also present in CMKC, have relatively little impact on platelet adhesion and aggregation (Dorahy, Thorne, Fecondo, & Burns, 1997; Wilner, Nossel, & LeRoy, 1968). However, studies have shown that negatively charged surfaces can activate factor XII and platelet factor 3, leading to intrinsic blood coagulation (Tranquilan-Aranilla, Barba, Vista, & Abad, 2016). We suggest that the processes that lead to platelet adhesion and activation on CMKC-containing nanofibers are related to attachment of plasma proteins and interactions of the platelets with these proteins attached to the nanofibers (Rodrigues, Gonçalves, Martins, Barbosa, & Ratner, 2006). Since this work used PRP, all the proteins present on the plasma (such as fibrinogen and complement

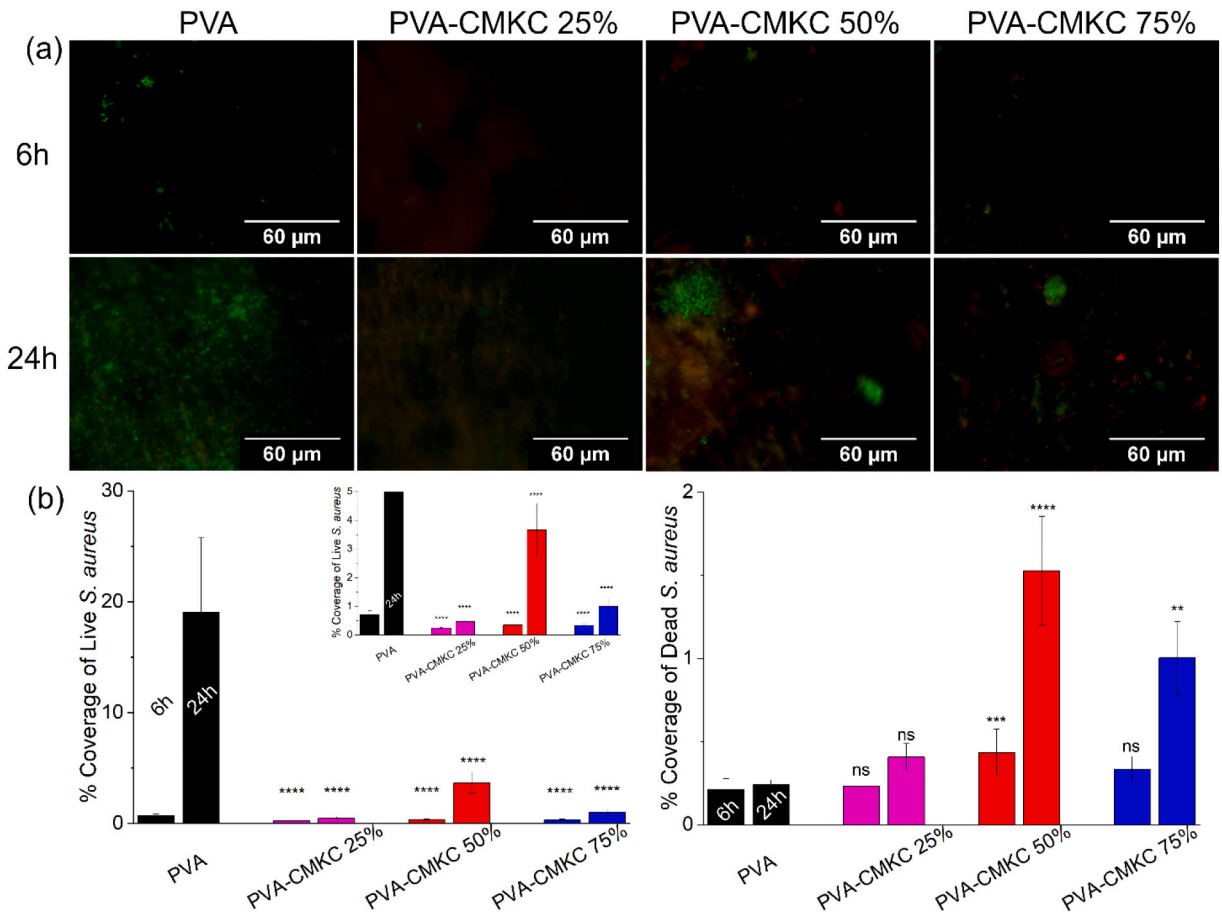


**Fig. 5.** Fluorescence microscopy images of *S. aureus* on the nanofibers. Live bacteria are represented in green (SYTO 9 stain) and dead bacteria in red (propidium iodide stain) (a). Percentage of coverage for live and dead *S. aureus* adhered to the nanofibers (b). Inset shows the percentage of coverage for live bacteria on an expanded y-axis for comparison. ****$p \leq 0.0001$, ***$p \leq 0.001$, **$p \leq 0.01$, and "ns" $p \geq 0.05$ compared to the PVA control.

proteins) can attach to the nanofibers and provide sites for the platelets to interact and attach. The presence of fibrinogen on the nanofibers shown on Fig. 1 and Table 2 corroborates these results. Data from the literature shows that fibrinogen adsorption is related to high platelet adhesion and activation and the conformation of the protein is relevant to this mechanism (Chiumiento, Lamponi, & Barbucci, 2007; Rodrigues, Gonçalves, Martins, Barbosa, & Ratner, 2006). Zhang et al. (2017) observed that on hydrophilic surfaces the γ400–411 platelet-binding dodecapeptide on the D region of fibrinogen is exposed, leading to formation of uniform monolayers of activated platelets on the surface (Zhang et al., 2017). Similar phenomena could be responsible for the observed platelet activation on the CMKC nanofibers reported here. In addition, the similarity of CMKC to biological molecules can promote biochemical signals and sites for the deposition and activation of platelets (Merkle et al., 2015b). Increasing the amount of CMKC to 75% made the fibers more unstable, due to the high presence of charges in solution when electrospinning, resulting in the highest fiber roughness and fiber porosity, and perhaps lower surface area for protein adsorption and subsequent platelet adhesion. This explains why the nanofibers with 75% CMKC presented lower number of platelets adhered, when compared to the ones with 50% CMKC. This trend also correlates to the higher amount of albumin and lower amount of fibrinogen on the 75% CMKC samples, compared to the 50% CMKC samples. Nonetheless, the difference in area of adhered platelets between the 50% and 75% CMKC nanofibers is not statistically significant.

### 3.2.3. Whole blood clotting

Blood clotting tests using human blood (plasma and erythrocytes) characterize the biochemical reactions involved in the hemostatic response. Although the investigation of single components of the coagulation cascade can provide information on specific interactions between blood components and the biomaterial, whole blood clotting offers the most accurate and clinically relevant thrombogenicity index, presenting the combined effects of all components (Sabino & Popat, 2020).

Human blood droplets were applied to the nanofibers and the clot formation after 15 and 30 min were analysed by absorbance measurements of the samples for the free hemoglobin released from the unclotted blood (Fig. 4). The blood clotting index (BCI) was calculated for all samples and the values of a blood sample in water at time 0 (as soon as the blood is collected) (Barba et al., 2018; Zhao et al., 2018). Absorbance measurements were scaled from 0% to 100% free hemoglobin. According to the absorbance values, the percentage of free hemoglobin for each sample was calculated and reported as blood clotting index, as shown in Fig. 4. A reduction in the free hemoglobin indicates an increase in the procoagulant activity. These results agree with the results from serum protein adsorption and from platelet adhesion and activation. All nanofiber samples exhibit some non-zero pro-coagulation activity; nanofibers with higher CMKC content (50 and 75%) resulted in significantly lower BCI than PVA nanofibers, reaching values close to 20%, with no statistically significant difference between the two. Therefore both the nanoscale features of the fibers and their chemistry promote coagulation (Vögtle et al., 2019; Xu, Weng, Gilkerson, Materon, & Lozano, 2015). The hemostatic effects of CMKC hydrogels are similar to the ones observed in CMKC nanofibers in terms of BCI and platelet adhesion, confirming the contribution of CMKC to the hemostatic

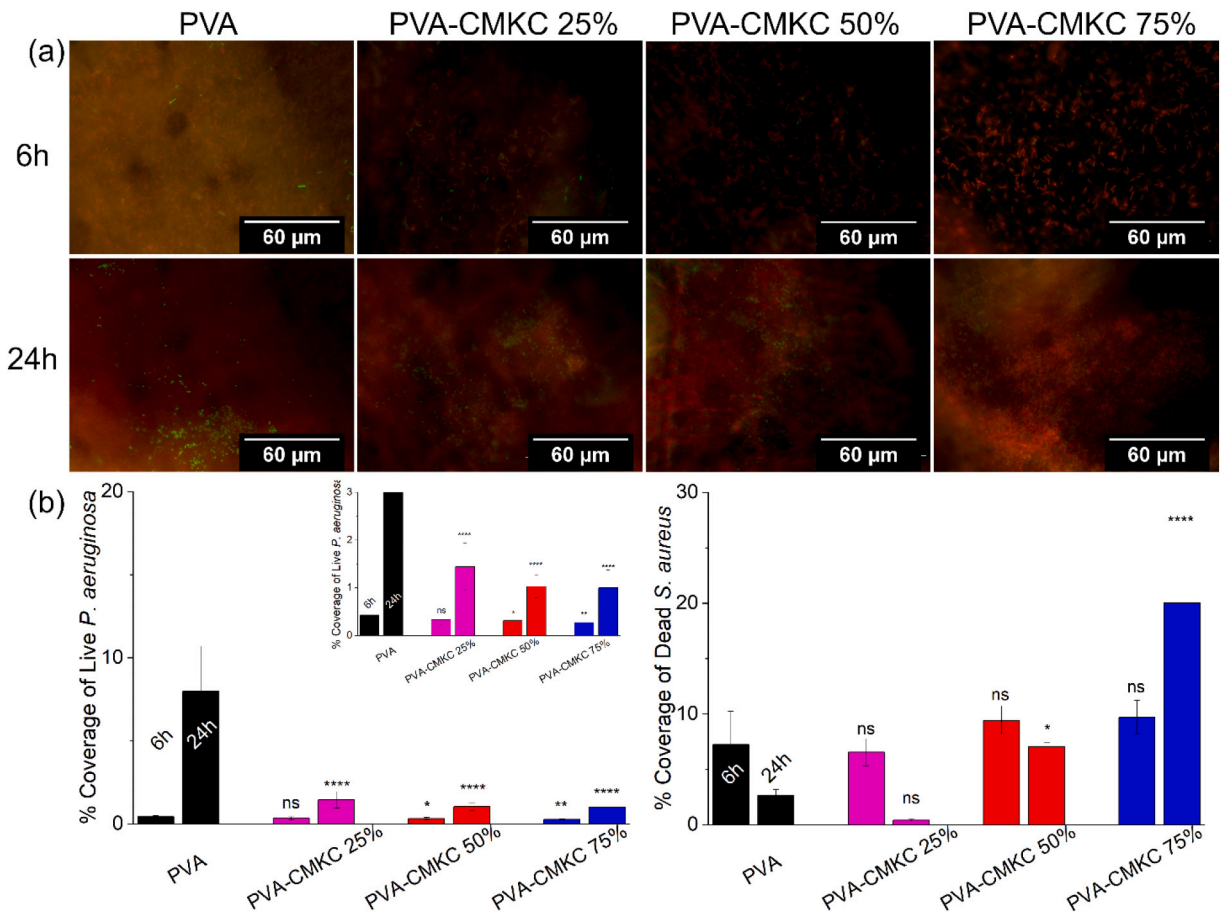


**Fig. 6.** Fluorescence microscopy images of *P. aeruginosa* on the nanofibers. Live bacteria are represented in green (SYTO 9 stain) and dead bacteria in red (propidium iodide stain) (a). Percentage of coverage for live and dead *S. aureus* adhered to the nanofibers (b). Inset shows the percentage of coverage for live bacteria on an expanded y-axis for comparison. ****$p \leq 0.0001$, **$p \leq 0.01$, *$p \leq 0.05$ and "ns" $p \geq 0.05$, compared to the PVA control.

behavior (Tranquilan-Aranilla, Barba, Vista, & Abad, 2016). CMKC-containing nanofibers with greater than 50% CMKC are strong candidates for application in wound dressings based on the observed procoagulant activity.

### 3.3. Antibacterial activity

#### 3.3.1. Bacteria adhesion on the nanofibers

Exposed wounds are viable environments for the colonization of bacteria, especially those present on the skin. Wound dressings that can repel or kill bacteria can help obviate the overuse of antibiotics (Vallet-Regí, González, & Izquierdo-Barba, 2019). Fluorescence images were used to assess the bacteria that were deposited on the nanofibers. The green dye (SYTO9) permeates the bacterial membranes, indicating live bacteria, while the red dye (propidium iodide), does not permeate live bacteria, only staining the bacteria that have some defect or failure in their membrane, staining only dead bacteria (Stiefel, Schmidt-Emrich, Maniura-Weber, & Ren, 2015). Quantifying bacterial adhesion is preferable over zone-of-inhibition tests on the nanofibers, due to the similarity with the conditions in a wound bed. The antibacterial effect observed here is not due to the release and diffusion of an antibacterial agent (measured by the zone-of-inhibition test). Rather, the antimicrobial activity is present on the fiber surface, making the evaluation of live/dead bacteria on the surface and bacterial morphology ideal for this material. Figs. 5 and 6 show fluorescence microscopy images and percentage coverage of live and dead *S. aureus* and *P. aeruginosa*, respectively, on the nanofibers after 6 h and 24 h. *S. aureus* is a coccal (round) Gram-positive bacterium, with a thick peptidoglycan-rich cell wall. Conversely, *P. aeruginosa* is a Gram-negative, bacillus (rod-shaped), with a complex and thin cell wall. In general, higher adhesion of *P. aeruginosa* bacteria is observed in all nanofibers, compared to *S. aureus*, which can be explained by the greater mobility of the bacteria, due to their flagella (Fredua-Agyeman, Gaisford, & Beezer, 2018). Despite the higher adhesion on the nanofibers, after 6 h of growth, almost all the *P. aeruginosa* adhered to the CMKC-containing nanofibers were stained red, which characterizes dead bacteria. After 24 h, the PVA nanofibers have a significant increase in the amount of live bacteria for both bacteria types. The CMKC-containing nanofibers with higher CMKC content have reduced live bacteria compared to the PVA nanofibers after 24 h for both types of bacteria. Furthermore, the 50% and 75% CMKC nanofibers have an increased number of dead bacteria compared to the PVA nanofibers after 24 h for both bacteria. Therefore, the CMKC-containing nanofibers do not provide a favorable environment for bacteria, even in a nutrient-rich broth condition.

#### 3.3.2. Bacteria morphology and biofilm formation

SEM images of the nanofibers after 6 and 24 h of incubation in bacteria broth were used to evaluate the morphology of adhered bacteria and biofilm formation. The images agree with the results from fluorescence microscopy. After 6 h, adhered *S. aureus* on the nanofibers (Fig. S4 — supplementary information) have a spherical morphology similar to "grape bunches," characteristic of *Staphylococcus*, and CMKC-containing nanofibers show a lower number of bacteria attached compared to PVA. Moreover, some bacteria on CMKC 75% nanofibers begin to exhibit morphological changes. After 24 h, PVA nanofibers show a high number of adhered *S. aureus* (Fig. 7), as well as colony

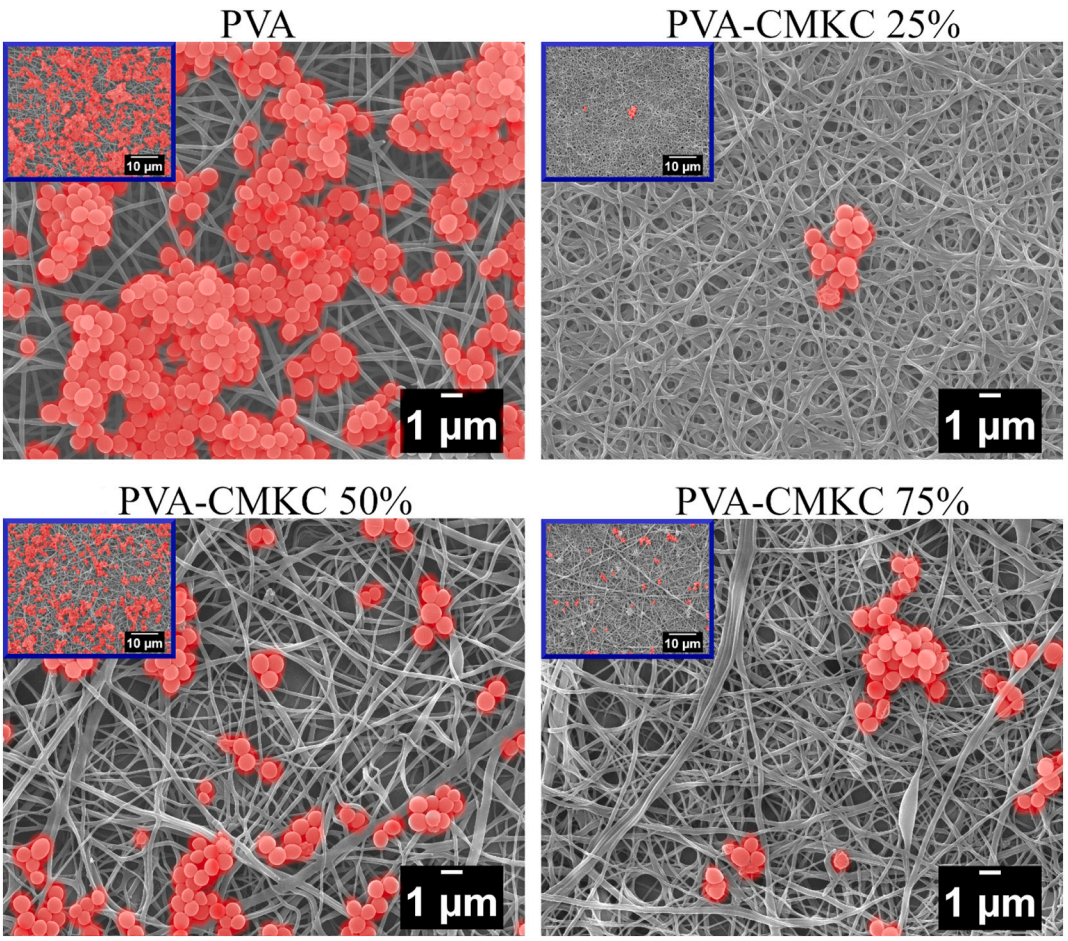


**Fig. 7.** False colored SEM images of *S. aureus* on the nanofibers after 24 h of incubation.

formation and aggregation. PVA-CMKC nanofibers show a low number of adhered bacteria and few colony formations, except on 50% CMKC, which may be due to the higher hydrophilicity. Confirming the fluorescence microscopy data, some bacteria on CMKC-containing fibers have an elliptical shape, and some defective membranes. These bacteria are probably dead. No biofilm formation was observed on any of the fibers.

It is important to note that *P. aeruginosa* is a biofilm-forming bacteria, a defense mechanism that makes it a pathogen that is difficult to fight (Madruga et al., 2020; Reynolds & Neufeld, 2016). After 6 h, adhered *P. aeruginosa* on the nanofibers (Fig. S5 — supplementary information) have a bacillus morphology, and all nanofibers have a high number of bacteria attached. However, some disruptions of the morphology can be observed, indicating dead bacteria. After 24 h, PVA nanofibers show a higher number of adhered *P. aeruginosa* (Fig. 8), as well as colony formation and some biofilm formation. PVA-CMKC nanofibers also have bacteria attached, but with defective morphology and no biofilm formation, corroborating the fluorescence microscopy and indicating significant antimicrobial activity.

CMKC-containing nanofibers have multiple features that may impart antibacterial activity. Because they have rigid cell walls, gram-positive and gram-negative bacteria cannot adapt easily to the nanoscale features, which can lead to cell death on nanostructured surfaces (Vallet-Regí, González, & Izquierdo-Barba, 2019). The increased hydrophilicity introduced by crosslinking the PVA with CMKC can promote the formation of a water layer on the surface, generating a physical and energetic barrier for the deposition of bacteria (Wang, Hu, & Shao, 2017). The charged carboxylate and sulfate groups in CMKC can also interact with the bacterial cell wall and membrane, affecting ion channels and respiratory enzymes, as well as the integrity of the membrane itself, causing the death of the bacteria (Pajerski et al., 2019).

## 4. Conclusions

In this study, electrospun PVA-CMKC nanofibers show enhanced blood coagulation and antibacterial activity, compared to PVA nanofibers. PVA-CMKC nanofibers preferentially adsorb fibrinogen compared to albumin, promote platelet adhesion and activation, and promote coagulation in contact with human whole blood. CMKC-containing nanofibers also exhibit superior antibacterial activity against both *Staphylococcus aureus* and *Pseudomonas aeruginosa* compared to PVA nanofibers. These favorable biological properties can be modulated by tuning the CMKC content. These properties are achieved due to a combination of the nanometer-scale features of the fibers and the biologically active biopolymer containing carboxyl, ether, and sulfate groups. PVA-CMKC nanofibers are non-cytotoxic, biodegradable, low-cost, and prepared following green manufacturing methods. PVA-CMKC nanofibers show potential for application as dressings for wound healing applications.

## CRediT authorship contribution statement

**Liszt Y.C. Madruga:** Conceptualization, Methodology, Validation, Formal analysis, Investigation, Data curation, Writing – original draft, Writing – review & editing, Visualization, Funding acquisition. **Ketul C. Popat:** Conceptualization, Resources, Writing – review & editing. **Rosangela C. Balaban:** Conceptualization, Methodology, Resources, Writing – review & editing, Supervision, Project administration,

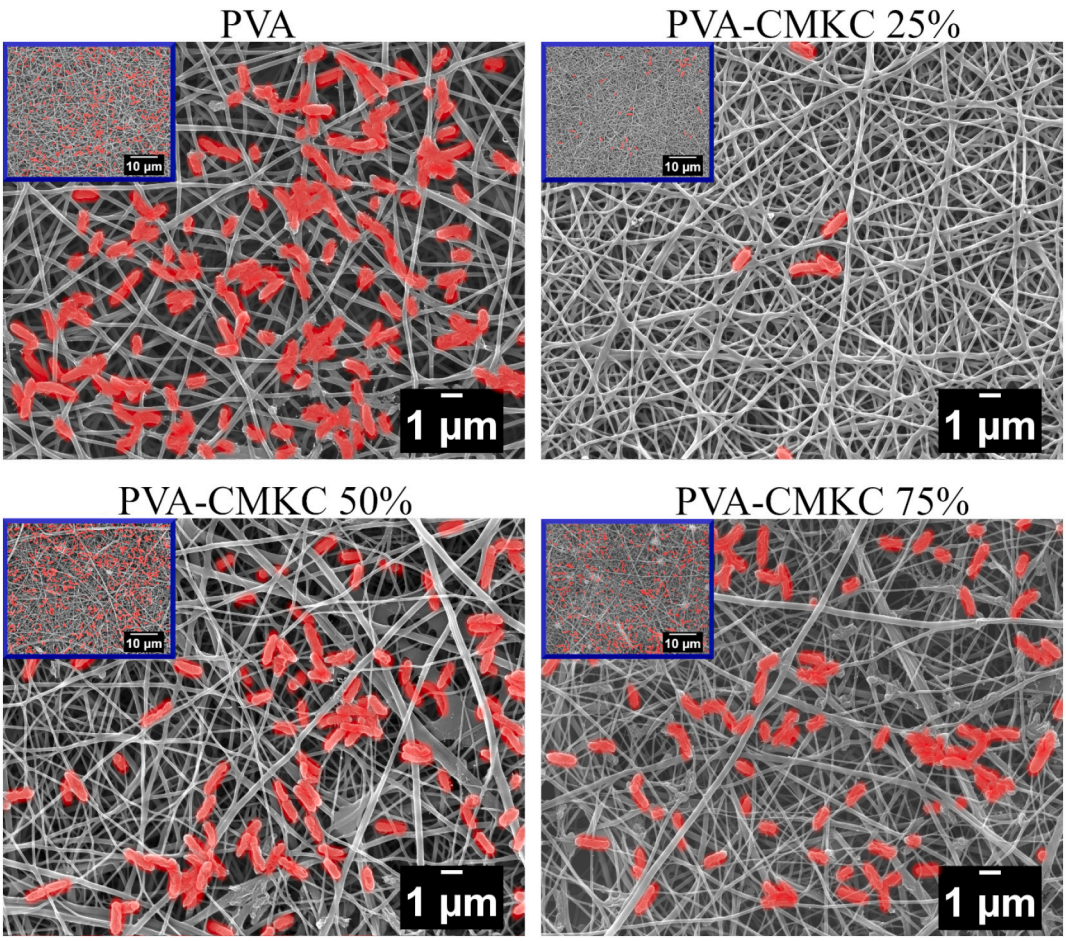


**Fig. 8.** False colored SEM images of *P. aeruginosa* on the nanofibers after 24 h of incubation.

Funding acquisition. **Matt J. Kipper:** Conceptualization, Methodology, Resources, Writing – review & editing, Supervision, Project administration, Funding acquisition.

## Acknowledgements

This study was financed in part by the Coordenação de Aperfeiçoamento de Pessoal de Nível Superior – Brasil (CAPES) – Finance Code 001. Also, the authors gratefully acknowledge the financial support from the National Science Foundation (award number 1933552).

## Appendix A. Supplementary data

Supplementary data to this article can be found online at https://doi.org/10.1016/j.carbpol.2021.118541.

## References

Almodóvar, J., Mower, J., Banerjee, A., Sarkar, A. K., Ehrhart, N. P., & Kipper, M. J. (2013). Chitosan-heparin polyelectrolyte multilayers on cortical bone: Periosteum-mimetic, cytophilic, antibacterial coatings. *Biotechnology and Bioengineering, 110*(2), 609–618. https://doi.org/10.1002/bit.24710

Bajpai, S. K., & Daheriya, P. (2014). Kappa-carrageenan/PVA films with antibacterial properties: Part 1. Optimization of preparation conditions and preliminary drug release studies. *Journal of Macromolecular Science, Part A, 51*(4), 286–295. https://doi.org/10.1080/10601325.2014.882687

Barba, B. J. D., Aranilla, C. T., Relleve, L. S., Cruz, V. R. C., Vista, J. R., & Abad, L. V. (2018). Hemostatic granules and dressing prepared from formulations of carboxymethyl cellulose, kappa-carrageenan and polyethylene oxide crosslinked by gamma radiation. *Radiation Physics and Chemistry, 144*(August 2017), 180–188. https://doi.org/10.1016/j.radphyschem.2017.08.009

Bhattacharjee, A., Clark, R., Gentry-Weeks, C., & Li, Y. V. (2020). A novel receptor-free polydiacetylene nanofiber biosensor for detecting *E. coli* via colorimetric changes. *Materials Advances, 1*(9), 3387–3397. https://doi.org/10.1039/D0MA00619J

da Câmara, P. C. F., Madruga, L. Y. C., Sabino, R. M., Vlcek, J., Balaban, R. C., Popat, K. C., … Kipper, M. J. (2020). Polyelectrolyte multilayers containing a tannin derivative polyphenol improve blood compatibility through interactions with platelets and serum proteins. *Materials Science and Engineering: C, 112*(March), Article 110919. https://doi.org/10.1016/j.msec.2020.110919

Chattopadhyay, S., & Raines, R. T. (2014). Collagen-based biomaterials for wound healing. *Biopolymers, 101*(8), 821–833. https://doi.org/10.1002/bip.22486

Chiumiento, A., Lamponi, S., & Barbucci, R. (2007). Role of fibrinogen conformation in platelet activation. *Biomacromolecules, 8*(2), 523–531. https://doi.org/10.1021/bm060664m

da Cruz, J. A., da Silva, A. B., Ramin, B. B. S., Souza, P. R., Popat, K. C., Zola, R. S., … Martins, A. F. (2020). Poly(vinyl alcohol)/cationic tannin blend films with antioxidant and antimicrobial activities. *Materials Science and Engineering C, 107* (August 2019), Article 110357. https://doi.org/10.1016/j.msec.2019.110357

Das, A., Abas, M., Biswas, N., Banerjee, P., Ghosh, N., Rawat, A., … Sen, C. K. (2019). A modified collagen dressing induces transition of inflammatory to reparative phenotype of wound macrophages. *Scientific Reports, 9*(1), 1–10. https://doi.org/10.1038/s41598-019-49435-z

do Nascimento Marques, N., dos Santos Alves, K., Vidal, R. R. L., da Silva Maia, A. M., Madruga, L. Y. C., Curti, P. S., … Taft, C. (2020). Chemical modification of polysaccharides and applications in strategic areas. In *Emerging research in science and engineering based on advanced experimental and computational strategies. Engineering materials* (pp. 433–472). Cham: Springer. https://doi.org/10.1007/978-3-030-31403-3_17.

Dorahy, D. J., Thorne, R. F., Fecondo, J. V., & Burns, G. F. (1997). Stimulation of platelet activation and aggregation by a carboxyl-terminal peptide from thrombospondin binding to the integrin-associated protein receptor. *Journal of Biological Chemistry, 272*(2), 1323–1330. https://doi.org/10.1074/jbc.272.2.1323

Dumont, M., Villet, R., Guirand, M., Montembault, A., Delair, T., Lack, S., Barikosky, M., Crepet, A., Alcouffe, P., Laurent, F., & David, L. (2018). Processing and antibacterial properties of chitosan-coated alginate fibers. *Carbohydrate Polymers, 190*(December 2016), 31–42. https://doi.org/10.1016/j.carbpol.2017.11.088

Fahimirad, S., & Ajalloueian, F. (2019). Naturally-derived electrospun wound dressings for target delivery of bio-active agents. *International Journal of Pharmaceutics, 566* (May), 307–328. https://doi.org/10.1016/j.ijpharm.2019.05.053

Felgueiras, H. P., & Amorim, M. T. P. (2017). Functionalization of electrospun polymeric wound dressings with antimicrobial peptides. *Colloids and Surfaces B: Biointerfaces, 156*, 133–148. https://doi.org/10.1016/j.colsurfb.2017.05.001

Fredua-Agyeman, M., Gaisford, S., & Beezer, A. E. (2018). Observation with microcalorimetry: Behaviour of *P. aeruginosa* in mixed cultures with *S. aureus* and *E. coli*. *Thermochimica Acta, 663*(March), 93–98. https://doi.org/10.1016/j.tca.2018.03.009

Fujiwara, T., Nishimoto, S., Ishise, H., Kawai, K., Fukuda, K., & Kakibuchi, M. (2012). Comparative study of the antibacterial penetrating effects of wound dressings. *Journal of Plastic Surgery and Hand Surgery, 46*(1), 2–7. https://doi.org/10.3109/2000656X.2011.644939

Guo, J., Zhou, H., Akram, M. Y., Mu, X., Nie, J., & Ma, G. (2016). Characterization and application of chondroitin sulfate/polyvinyl alcohol nanofibres prepared by electrospinning. *Carbohydrate Polymers, 143*, 239–245. https://doi.org/10.1016/j.carbpol.2016.02.013

Haider, A., Haider, S., & Kang, I.-K. (2018). A comprehensive review summarizing the effect of electrospinning parameters and potential applications of nanofibers in biomedical and biotechnology. *Arabian Journal of Chemistry, 11*(8), 1165–1188. https://doi.org/10.1016/j.arabjc.2015.11.015

Hedayati, M., Neufeld, M. J., Reynolds, M. M., & Kipper, M. J. (2019). The quest for blood-compatible materials: Recent advances and future technologies. *Materials Science and Engineering: R: Reports, 138*(July), 118–152. https://doi.org/10.1016/j.mser.2019.06.002

Homaeigohar, S., & Boccaccini, A. R. (2020). Antibacterial biohybrid nanofibers for wound dressings. *Acta Biomaterialia, 107*(2020), 25–49. https://doi.org/10.1016/j.actbio.2020.02.022

Krauel, K., Hackbarth, C., Fürll, B., & Greinacher, A. (2012). Heparin-induced thrombocytopenia: In vitro studies on the interaction of dabigatran, rivaroxaban, and low-sulfated heparin, with platelet factor 4 and anti-PF4/heparin antibodies. *Blood, 119*(5), 1248–1255. https://doi.org/10.1182/blood-2011-05-353391

Ma, N., Liu, X.-W., Yang, Y.-J., Li, J.-Y., Mohamed, I., Liu, G.-R., & Zhang, J.-Y. (2015). Preventive effect of aspirin eugenol ester on thrombosis in κ-carrageenan-induced rat tail thrombosis model. *PLoS One, 10*(7), Article e0133125. https://doi.org/10.1371/journal.pone.0133125

Madruga, L. Y. C., Balaban, R. C., Popat, K. C., & Kipper, M. J. (2021). Biocompatible crosslinked nanofibers of poly(vinyl alcohol)/carboxymethyl-kappa-carrageenan produced by a green process. *Macromolecular Bioscience, 21*(1), Article 2000292. https://doi.org/10.1002/mabi.202000292

Madruga, L. Y. C., da Câmara, P. C. F., Marques, N.d. N., & Balaban, R.d. C. (2018). Effect of ionic strength on solution and drilling fluid properties of ionic polysaccharides: A comparative study between Na-carboxymethylcellulose and Na-kappa-carrageenan responses. *Journal of Molecular Liquids, 266*, 870–879. https://doi.org/10.1016/j.molliq.2018.07.016

Madruga, L. Y. C., Sabino, R. M., Santos, E. C. G., Popat, K. C., Balaban, R.d. C., & Kipper, M. J. (2020). Carboxymethyl-kappa-carrageenan: A study of biocompatibility, antioxidant and antibacterial activities. *International Journal of Biological Macromolecules, 152*, 483–491. https://doi.org/10.1016/j.ijbiomac.2020.02.274

Merkle, V. M., Martin, D., Hutchinson, M., Tran, P. L., Behrens, A., Hossainy, S., … Slepian, M. J. (2015a). Hemocompatibility of poly(vinyl alcohol)-gelatin core-shell electrospun nanofibers: A scaffold for modulating platelet deposition and activation. *ACS Applied Materials and Interfaces, 7*(15), 8302–8312. https://doi.org/10.1021/acsami.5b01671

Merkle, V. M., Martin, D., Hutchinson, M., Tran, P. L., Behrens, A., Hossainy, S., … Slepian, M. J. (2015b). Hemocompatibility of poly(vinyl alcohol)–gelatin core–shell electrospun nanofibers: A scaffold for modulating platelet deposition and activation. *ACS Applied Materials & Interfaces, 7*(15), 8302–8312. https://doi.org/10.1021/acsami.5b01671

Miguel, S. P., Figueira, D. R., Simões, D., Ribeiro, M. P., Coutinho, P., Ferreira, P., & Correia, I. J. (2018). Electrospun polymeric nanofibres as wound dressings: A review. *Colloids and Surfaces B: Biointerfaces, 169*, 60–71. https://doi.org/10.1016/j.colsurfb.2018.05.011

Mogoşanu, G. D., & Grumezescu, A. M. (2014). Natural and synthetic polymers for wounds and burns dressing. *International Journal of Pharmaceutics, 463*(2), 127–136. https://doi.org/10.1016/j.ijpharm.2013.12.015

Nas, F. S., Abrigo, M., McArthur, S. L., & Kingshott, P. (2014). Electrospun nanofibers as dressings for chronic wound care: Advances, challenges, and future prospects. *Macromolecular Bioscience, 14*(6), 772–792. https://doi.org/10.1002/mabi.201300561

de Oliveira, M., Madruga, L., de Lima, B., Villetti, M., de Souza Filho, M., Kipper, M., … Balaban, R. (2021). Agro-industrial waste valorization: Transformation of starch from mango kernel into biocompatible, thermoresponsive and high swelling nanogels. *Journal of the Brazilian Chemical Society, 00*(00), 1–10. https://doi.org/10.21577/0103-5053.20210059

Paar, M., Rossmann, C., Nusshold, C., Wagner, T., Schlagenhauf, A., Leschnik, B., … Hallström, S. (2017). Anticoagulant action of low, physiologic, and high albumin levels in whole blood. *PLoS One, 12*(8), 1–12. https://doi.org/10.1371/journal.pone.0182997

Pajerski, W., Ochonska, D., Brzychczy-Wloch, M., Indyka, P., Jarosz, M., Golda-Cepa, M., Sojka, Z., & Kotarba, A. (2019). Attachment efficiency of gold nanoparticles by Gram-positive and Gram-negative bacterial strains governed by surface charges. *Journal of Nanoparticle Research, 21*(8). https://doi.org/10.1007/s11051-019-4617-z

Prawel, D. A., Dean, H., Forleo, M., Lewis, N., Gangwish, J., Popat, K. C., … James, S. P. (2014). Hemocompatibility and hemodynamics of novel hyaluronan–polyethylene materials for flexible heart valve leaflets. *Cardiovascular Engineering and Technology, 5*(1), 70–81. https://doi.org/10.1007/s13239-013-0171-5

Reynolds, B. H. N. M., & Neufeld, B. H. (2016). *Critical nitric oxide concentration for Pseudomonas aeruginosa biofilm reduction on polyurethane substrates*, Article 031012. https://doi.org/10.1116/1.4962266

Rodrigues, S. N., Gonçalves, I. C., Martins, M. C. L., Barbosa, M. A., & Ratner, B. D. (2006). Fibrinogen adsorption, platelet adhesion and activation on mixed hydroxyl-/methyl-terminated self-assembled monolayers. *Biomaterials, 27*(31), 5357–5367. https://doi.org/10.1016/j.biomaterials.2006.06.010

Sabino, R. M., Kauk, K., Madruga, L. Y. C., Kipper, M. J., Martins, A. F., & Popat, K. C. (2020). Enhanced hemocompatibility and antibacterial activity on titania nanotubes with tanfloc/heparin polyelectrolyte multilayers. *Journal of Biomedical Materials Research — Part A, 108*(4), 992–1005. https://doi.org/10.1002/jbm.a.36876

Sabino, R. M., Kauk, K., Movafaghi, S., Kota, A., & Popat, K. C. (2019). Interaction of blood plasma proteins with superhemophobic titania nanotube surfaces. *Nanomedicine: Nanotechnology, Biology and Medicine, 21*, Article 102046. https://doi.org/10.1016/j.nano.2019.102046

Sabino, R. M., & Popat, K. C. (2020). Evaluating whole blood clotting in vitro on biomaterial surfaces. *Bio-Protocol, 10*(3), Article e3505. https://doi.org/10.21769/BioProtoc.3505

Sadeghi, A., Zandi, M., Pezeshki-Modaress, M., & Rajabi, S. (2019). Tough, hybrid chondroitin sulfate nanofibers as a promising scaffold for skin tissue engineering. *International Journal of Biological Macromolecules, 132*, 63–75. https://doi.org/10.1016/j.ijbiomac.2019.03.208

Simon-Walker, R., Romero, R., Staver, J. M., Zang, Y., Reynolds, M. M., Popat, K. C., & Kipper, M. J. (2017). Glycocalyx-inspired nitric oxide-releasing surfaces reduce platelet adhesion and activation on titanium. *ACS Biomaterials Science & Engineering, 3*(1), 68–77. https://doi.org/10.1021/acsbiomaterials.6b00572

Sivaraman, B., & Latour, R. A. (2010). The relationship between platelet adhesion on surfaces and the structure versus the amount of adsorbed fibrinogen. *Biomaterials, 31*(5), 832–839. https://doi.org/10.1016/j.biomaterials.2009.10.008

Stiefel, P., Schmidt-Emrich, S., Maniura-Weber, K., & Ren, Q. (2015). Critical aspects of using bacterial cell viability assays with the fluorophores SYTO9 and propidium iodide. *BMC Microbiology, 15*(1), 36. https://doi.org/10.1186/s12866-015-0376-x

Tranquilan-Aranilla, C., Barba, B. J. D., Vista, J. R. M., & Abad, L. V. (2016). Hemostatic efficacy evaluation of radiation crosslinked carboxymethyl kappa-carrageenan and chitosan with varying degrees of substitution. *Radiation Physics and Chemistry, 124*, 124–129. https://doi.org/10.1016/j.radphyschem.2016.02.003

Trinca, R. B., Westin, C. B., da Silva, J. A. F., & Moraes, Â. M. (2017). Electrospun multilayer chitosan scaffolds as potential wound dressings for skin lesions. *European Polymer Journal, 88*, 161–170. https://doi.org/10.1016/j.eurpolymj.2017.01.021

Truong, Y. B., Glattauer, V., Briggs, K. L., Zappe, S., & Ramshaw, J. A. M. (2012). Collagen-based layer-by-layer coating on electrospun polymer scaffolds. *Biomaterials, 33*(36), 9198–9204. https://doi.org/10.1016/j.biomaterials.2012.09.012

Unnithan, A. R., Sasikala, A. R. K., Murugesan, P., Gurusamy, M., Wu, D., Park, C. H., & Kim, C. S. (2015). Electrospun polyurethane-dextran nanofiber mats loaded with Estradiol for post-menopausal wound dressing. *International Journal of Biological Macromolecules, 77*, 1–8. https://doi.org/10.1016/j.ijbiomac.2015.02.044

Vallet-Regí, M., González, B., & Izquierdo-Barba, I. (2019). Nanomaterials as promising alternative in the infection treatment. *International Journal of Molecular Sciences, 20*(15). https://doi.org/10.3390/ijms20153806

Vlcek, J. R., Hedayati, M., Melvin, A. C., Reynolds, M. M., & Kipper, M. J. (2021). Blood-compatible materials: Vascular endothelium-mimetic surfaces that mitigate multiple cell-material interactions. *Advanced Healthcare Materials, 10*(7), Article 2001748. https://doi.org/10.1002/adhm.202001748

Vögtle, T., Sharma, S., Mori, J., Nagy, Z., Semeniak, D., Scandola, C., … Senis, Y. A. (2019). Heparan sulfates are critical regulators of the inhibitory megakaryocyte-platelet receptor G6b-B. *ELife, 8*, 1–43. https://doi.org/10.7554/eLife.46840

Wang, L., Hu, C., & Shao, L. (2017). The-antimicrobial-activity-of-nanoparticles—Present-situati. *International Journal of Nanomedicine, 12*, 1227–1249. https://doi.org/10.2147/IJN.S121956

Wilner, G. D., Nossel, H. L., & LeRoy, E. C. (1968). Aggregation of platelets by collagen. *Journal of Clinical Investigation, 47*(12), 2616–2621. https://doi.org/10.1172/JCI105944

Xu, F., Weng, B., Gilkerson, R., Materon, L. A., & Lozano, K. (2015). Development of tannic acid/chitosan/pullulan composite nanofibers from aqueous solution for potential applications as wound dressing. *Carbohydrate Polymers, 115*, 16–24. https://doi.org/10.1016/j.carbpol.2014.08.081

Yang, L., Han, L., Liu, Q., Xu, Y., & Jia, L. (2017). Galloyl groups-regulated fibrinogen conformation: Understanding antiplatelet adhesion on tannic acid coating. *Acta Biomaterialia, 64*, 187–199. https://doi.org/10.1016/j.actbio.2017.09.034

Yegappan, R., Selvaprithiviraj, V., Amirthalingam, S., & Jayakumar, R. (2018). Carrageenan based hydrogels for drug delivery, tissue engineering and wound healing. *Carbohydrate Polymers, 198*(June), 385–400. https://doi.org/10.1016/j.carbpol.2018.06.086

Young, B. M., Shankar, K., Allen, B. P., Pouliot, R. A., Schneck, M. B., Mikhaiel, N. S., & Heise, R. L. (2017). Electrospun decellularized lung matrix scaffold for airway smooth muscle culture. *ACS Biomaterials Science & Engineering, 3*(12), 3480–3492. https://doi.org/10.1021/acsbiomaterials.7b00384

Zahedi, P., Rezaeian, I., Ranaei-Siadat, S.-O., Jafari, S.-H., & Supaphol, P. (2010). A review on wound dressings with an emphasis on electrospun nanofibrous polymeric bandages. *Polymers for Advanced Technologies, 21*(2), 77–95. https://doi.org/10.1002/pat.1625

Zeng, Q., Qin, J., Yin, X., Liu, H., Zhu, L., Dong, W., & Zhang, S. (2016). Preparation and hemocompatibility of electrospun O-carboxymethyl chitosan/PVA nanofibers. *Journal of Applied Polymer Science, 133*(26), 2–9. https://doi.org/10.1002/app.43565

Zhang, L., Casey, B., Galanakis, D. K., Marmorat, C., Skoog, S., Vorvolakos, K., … Rafailovich, M. H. (2017). The influence of surface chemistry on adsorbed fibrinogen conformation, orientation, fiber formation and platelet adhesion. *Acta Biomaterialia, 54*, 164–174. https://doi.org/10.1016/j.actbio.2017.03.002

Zhao, R., Li, X., Sun, B., Zhang, Y., Zhang, D., Tang, Z., Chen, X., & Wang, C. (2014). Electrospun chitosan/sericin composite nanofibers with antibacterial property as potential wound dressings. *International Journal of Biological Macromolecules, 68*, 92–97. https://doi.org/10.1016/j.ijbiomac.2014.04.029

Zhao, X., Gao, J., Hu, X., Guo, H., Wang, F., Qiao, Y., & Wang, L. (2018). Collagen/polyethylene oxide nanofibrous membranes with improved hemostasis and cytocompatibility for wound dressing. *Applied Sciences, 8*(8), 1226. https://doi.org/10.3390/app8081226

Zia, K. M., Tabasum, S., Nasif, M., Sultan, N., Aslam, N., Noreen, A., & Zuber, M. (2017). A review on synthesis, properties and applications of natural polymer based carrageenan blends and composites. *International Journal of Biological Macromolecules, 96*, 282–301. https://doi.org/10.1016/j.ijbiomac.2016.11.095